

## Chapter 2

# Evolution and Breakdown of a Subsonic Round Jet

We begin with the dynamics of a round jet emphasizing the contribution of longitudinal disturbances to the perturbed flow pattern. Important issues are generation, spatial development, and interaction of the three-dimensional structures with the ring vortices. Supplementary material to this chapter is given by the multimedia files titled Chap. 2: “Multimedia files Nos. 2.1–2.8” (<http://extras.springer.com>).

### 2.1 Experimental Technique

A test facility used for modeling of the round jet was that with a Vitoshinsky nozzle, a settling chamber (1) and deturbulizing grids (2) as is shown in Fig. 2.1. The air stream in the channel is generated by a fan. In most of the experimental runs which were performed, the jet core velocity  $U_0$  at the nozzle exit of the diameter  $d = 40$  mm was equal to 4 m/s making the Reynolds number  $Re = U_0 d / \nu = 10,600$ . Experimental results presented in what follows were obtained by flow visualization and hot-wire measurements.

At the visualization, smoke was injected into the jet from the fan side. The flow patterns were recorded by a digital camera (9) providing a general view of the jet and its slices both in streamwise and cross sections through illumination of the flow by a laser sheet of 0.5 mm thickness (7). Also, the flow was illuminated by a light sheet of a filament lamp using a narrow slot of a diaphragm. To examine the effects of acoustic excitation, the jet was forced by a dynamic loudspeaker (8) generating harmonic oscillations at controlled variation of their frequency and sound pressure level. The acoustic forcing was also used to synchronize the rolling up of the Kelvin–Helmholtz ring vortices with the laser illumination periodically switched on for short time intervals to record stroboscopic patterns of the interaction between the ring vortices and the three-dimensional perturbations.

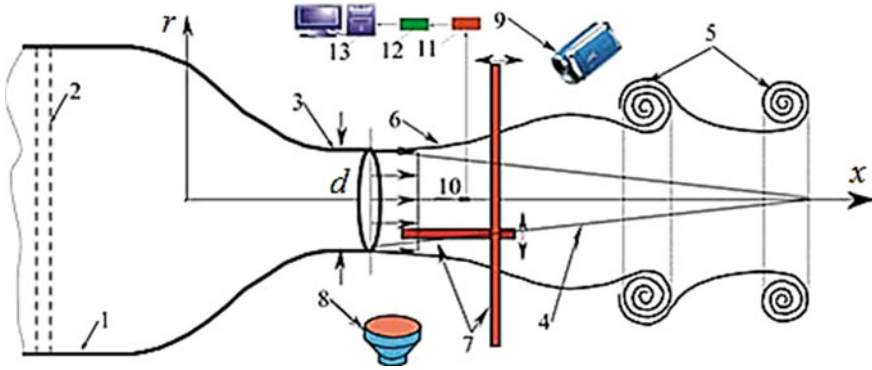


**Fig. 2.1** Experimental set-up: settling chamber (1), deturbulizing grids (2), nozzle (3), potential core of the jet (4), Kelvin-Helmholtz vortices (5), 3D disturbances (6), positions of the laser sheet (7), loudspeaker (8), digital camera (9), hot-wire probe (10), hot-wire anemometer (11), ADC (12), PC (13)

The hot-wire measurements of the streamwise mean velocity and fluctuations were performed with a DISA constant-temperature anemometer (11) and a one-wire probe of 1-mm length and 5- $\mu\text{m}$  diameter made of gilded tungsten (10). The probe was operated at 80 % overheat ratio and calibrated through the modified King's law

$$U = k_1(E^2 - E_0^2)^{1/n} + k_2(E - E_0)^{1/2},$$

where  $E$  and  $E_0$  are the output voltages of the anemometer at flow velocity switched on and off, respectively, and  $k_1$ ,  $k_2$ ,  $n$  are constants. The index  $1/n$  is usually about 2, the constant  $k_2$  allows for free convection near the wall where the flow velocity is close to zero. The maximum error at the probe calibration did not exceed 1 % of  $U_0$ . The hot-wire signal was digitized by a 16-bit analog-to-digital converter (12) for further acquisition and processing with a personal computer (13). The same technique applies to hot-wire results on other configurations of jet flows discussed in the following chapters.

## 2.2 Velocity Characteristics

Distributions of the mean and fluctuation velocity components at different streamwise distances from the nozzle exit are shown in Fig. 2.2. The jet was traversed by the hot-wire probe in four cross sections at  $x/d = 0.2, 0.3, 0.55$ , and  $0.8$  where  $x$  is the streamwise coordinate measured from the nozzle exit. In the figure, the radial distance  $r$  is normalized by the channel radius  $d/2$ , the mean flow velocity  $U$  and rms amplitude of disturbances  $u'$  are reduced by the maximum value  $U_0$  at the jet axis. The mean-flow profiles demonstrate a wide jet core and a narrow region

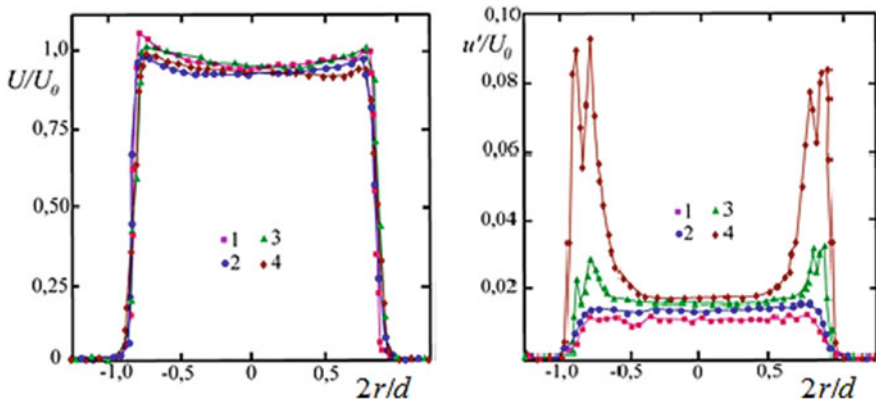


**Fig. 2.2** Radial distributions of the mean (*left*) and fluctuation (*right*) streamwise velocity components at different distances from the nozzle exit:  $x/d = 0.2$  (1), 0.3 (2), 0.55 (3), and 0.8 (4);  $U_0 = 4$  m/s

of strong velocity gradient at the jet periphery. Virtually, such distributions called “top-hat” profiles result in the generation of the ring vortices (Kelvin–Helmholtz ones) close the nozzle exit. A similar phenomenon is observed at the blowing of vortex rings by a tricky smoker. To do this, he draws an outward breath through the lips rounded off in the form of a nozzle and creates the velocity profile of the jet, similar to that presented in Fig. 2.2.

### 2.3 Interaction of the Primary Vortices with the Longitudinal Disturbances

An example of smoke visualization of the laminar jet breakdown at  $Re = 10,000$  is given by Van Dyke (1986) where one can observe the Kelvin–Helmholtz instability at the jet periphery. Then, this flow region rolls up into vortex rings and after that the jet suddenly becomes turbulent. The smoke ring looks like a tightly twisted toroidal helix appearing due to the roll up of the vortex sheet that comes off the nozzle edge. The transition of laminar jet to the turbulent state is primarily caused by the Kelvin–Helmholtz instability, and further, by the secondary instability of vortex rings. The latter, often called the Widnall instability, is also illustrated by Van Dyke (1986) and appears as growing waves around the vortex ring. The origination of these waves is usually explained by the interaction of the Kelvin–Helmholtz and the streamwise vortices produced using a specially profiled nozzle as well as appearing due to the secondary instability of the jet. The interaction of the longitudinal vortices generated by the jet secondary instabilities with the ring vortices is investigated in detail by Demare and Baillot (2001). They have shown that between the ring vortices there is an emission of longitudinal

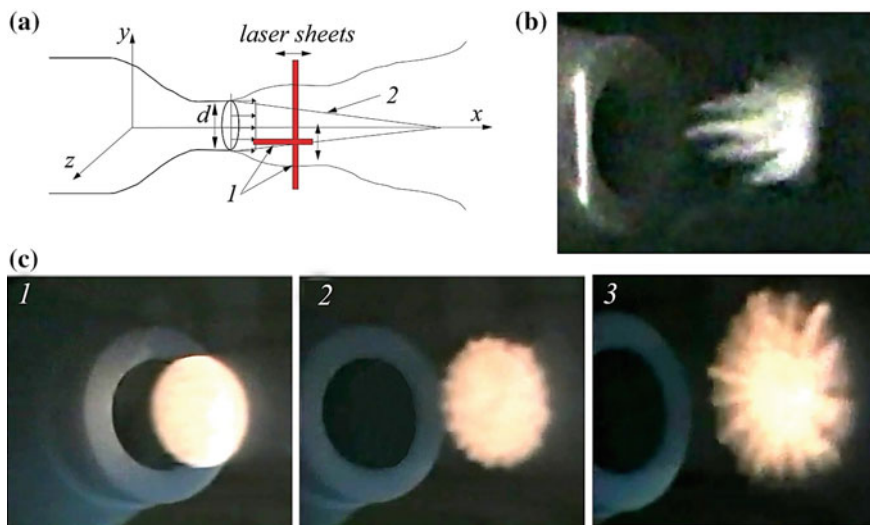


**Fig. 2.3** Natural longitudinal disturbances in the near field of the round jet: scheme of the jet illumination by thin light beams marked by 1 and 2 (a); flow pattern in the streamwise section at  $r/d = 0.4$  (b); the same in cross sections at  $x/d = 0.4$  (1),  $0.68$  (2), and  $0.86$  (3) (c);  $U_0 = 4$  m/s (see Presentation Chap. 2: “Multimedia files Nos. 2.1–2.4”) (<http://extras.springer.com>)

counter-rotating vortices in the azimuthal or radial direction. This leads to enhancement of the jet mixing with the surrounding air over the entire periphery of the jet.

The three-dimensional disturbances which are localized at the jet periphery and arise in natural conditions close to the nozzle exit are visualized using a light sheet as is shown in Fig. 2.3. In the present case, one expects several reasons for their origination including surface roughness, presence of grids and honeycombs in the settling chamber, etc. The streamwise evolution of the generated perturbations and their interaction with the ring vortices result in the jet turbulization.

Naturally occurring streamwise elongated perturbations are subject to radial oscillations complicating the observation of flow details. Therefore, they were modeled using controlled roughness elements, each of 0.2-mm height and 5-mm width, glued on the internal surface of the nozzle near its exit at their spacing correlating to the azimuthal scale of the natural perturbations. In this way, the development and interactions of the three-dimensional disturbances could be stabilized.

Visualization results in the form of stroboscopic patterns obtained with the laser sheet illumination illustrate the jet slices at different distances from the nozzle in Fig. 2.4. At the nozzle exit (Fig. 2.4b), the jet boundary is nearly sinusoidal along the full circumference. At  $x/d = 0.3$  (Fig. 2.4c) the sinusoidal contour is distorted by the azimuthal beams as a result of the interaction of the first ring vortex with the longitudinal perturbations generated at the roughness elements. Then, at  $x/d = 0.5$

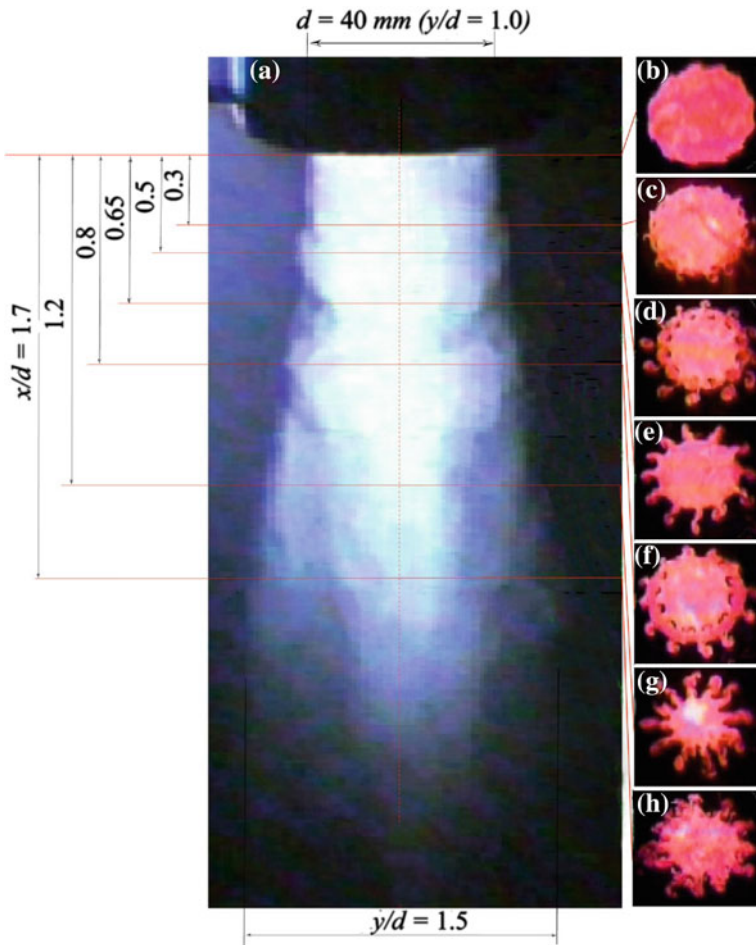


**Fig. 2.4** General view of the round jet (a) and its cross sections at different distances from the nozzle exit (b–h) (see Presentation Chap. 2: “Multimedia files Nos. 2.5–2.8”) (<http://extras.springer.com>)

(Fig. 2.4d), the distortion increases in the center of the first ring vortex, and the beams take the form of thin pins with the mushroom-like structures arising at their tips, similar to those described by Demare and Baillot (2001). These are identified as a pair of vortices rotating in opposite directions. In the region between the first and second ring vortices at  $x/d = 0.65$  (Fig. 2.4e), the ring vortices are not observed, but the intensity of beams increases. At  $x/d = 0.8$  (Fig. 2.4f), some dynamics of the beams is found, especially after the passage of the second ring vortex at  $x/d = 1.2$  (Fig. 2.4g). Then, while moving downstream, the intensive mixing of the jet with the surrounding air occurs through the development of the beams and, finally, the entire jet becomes almost turbulent at  $x/d = 1.7$  (Fig. 2.4h).

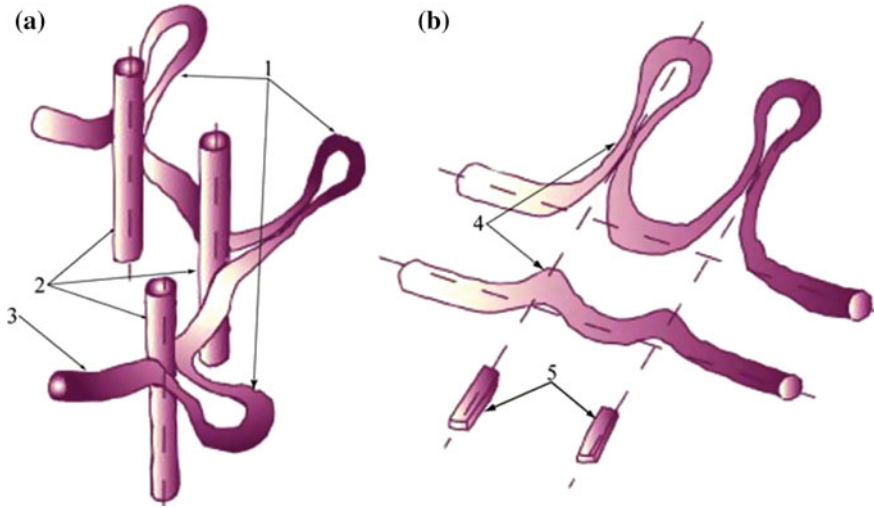
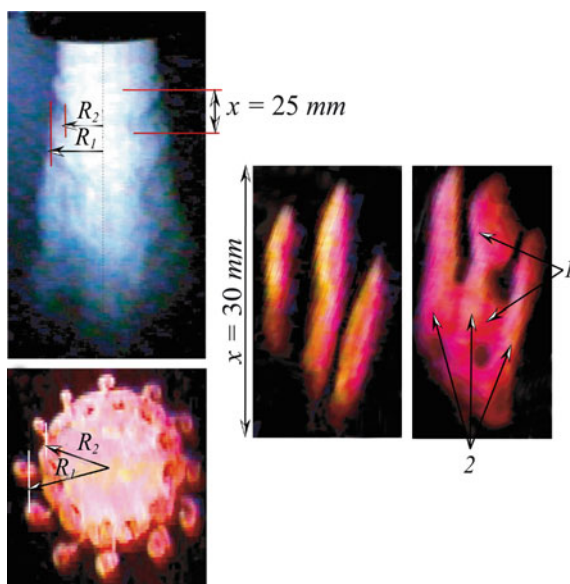


**Fig. 2.5** Three-dimensional deformation of the ring vortex (a) as compared to that of the Tollmien-Schlichting wave in a boundary layer (b):  $\Lambda$ - or  $\Omega$ -like vortices (1), longitudinal disturbances (2), ring vortex (3), 3D distortions of the 2D instability wave (4), roughness elements (5)

The above process of the laminar jet breakdown associated with the interaction of the three-dimensional disturbances with the ring vortices resembles the deformation of two-dimensional instability waves in boundary layers which is followed by generation of so-called  $\Lambda$ - or  $\Omega$ -like structures. In a boundary layer they appear as two vortices rotating in opposite directions with a “head” at their tips. In the classical experiment by Klebanoff et al. (1962) the  $\Lambda$ -structures were observed in a flat-plate flow at a distortion of the Tollmien–Schlichting wave by local boundary-layer non-uniformities. In the present case, such non-uniformities are the longitudinal perturbations as is sketched in Fig. 2.5. A two-dimensional ring vortex, while passing through the flow region perturbed by the longitudinal disturbances, interacts with them and undergoes a three-dimensional deformation which results in the characteristic bursts well seen all over the jet periphery. Those observed in Fig. 2.4 are likely to be the “heads” of  $\Lambda$ - or  $\Omega$ -like structures.

Note that in the boundary layer the  $\Lambda$ -structures start growing from the wall at local flow velocity close to zero towards the edge of the layer where the velocity tends to its external-flow value. Vice versa, in the jet two counter rotating vortices are ejected from the high-speed region of the vortex ring to surrounding air at rest so that the  $\Lambda$ -structure is elongated at its downstream propagation. Flow patterns taken in the region of the “heads” of  $\Lambda$ - or  $\Omega$ -like structures (at the radial distance  $R_1$ ) and at their origination from the ring vortex ( $R_2$ ) are presented in Fig. 2.6. Three smoke streaks are observed in the region of the “heads” (Fig. 2.6c). As is distinctly seen in Fig. 2.6d, their length is larger than the distance between two adjacent ring

**Fig. 2.6** General view of the round jet (a); a cross section (b); streamwise sections at  $R_1$  (c) and  $R_2$  (d); positions of the ring vortices and the longitudinal perturbations are marked by 1 and 2, respectively (see Presentation Chap. 2: “Multimedia files Nos. 2.5–2.7, 2.8”) (<http://extras.springer.com>)



vortices. Thus the streamwise elongated perturbations are likely spreading far downstream up to the jet turbulization.

## 2.4 High-Frequency Instability of the Longitudinal Perturbations

Inducing local velocity gradients in shear layers, the three-dimensional disturbances are often prone to high-frequency oscillations stimulating the laminar-turbulent transition. One expects that a similar phenomenon may have a valuable contribution to the round jet turbulization, as well. To clarify this point, an oscillatory disturbance was injected by periodic blowing/suction of air through a tiny hole at the nozzle surface near one of the roughness elements (Fig. 2.7). As a result, the three-dimensional flow perturbation associated with the element became more pronounced than is seen in the top of Fig. 2.7b (1). Further downstream, the neighboring longitudinal structures are also intensified being involved in the jet turbulization, see Fig. 2.7b (2). These observations indicate that the laminar jet breakdown can be controlled through the excitation of secondary instability of the streamwise elongated disturbances.



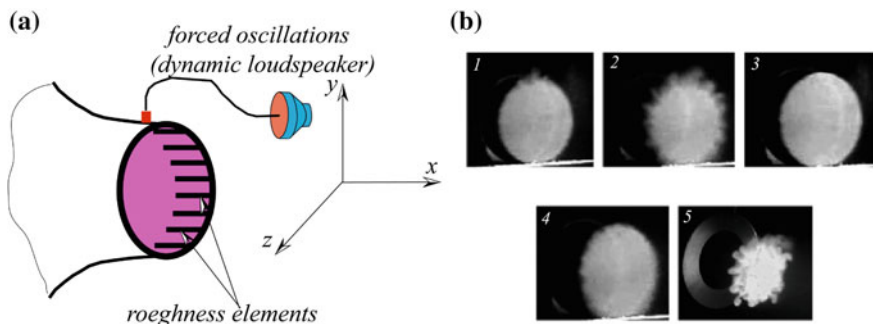


**Fig. 2.7** Secondary instability of the longitudinal structures: experimental scheme (a); cross sections of the jet at  $x/d = 0.2$  (1 and 3), 0.4 (2 and 4), and 0.68 (5); flow patterns 1, 2, and 5 are affected by the secondary disturbances while images 3 and 4 were taken in the absence of the forced oscillations (b);  $U_0 = 4$  m/s (see Presentation Chap. 2: “Multimedia file No. 2.4”) (<http://extras.springer.com>)

## 2.5 Jet Dynamics Under Acoustic Excitation

Two effects of the external acoustic forcing which can be involved in control of jet flows are just mentioned here. One of them is modification of the scale of the ring vortices. An example is given in Fig. 2.8 where the perturbed flow patterns visualized at variation of the excitation frequency can be compared.

Another effect to be emphasized is acoustic stimulation of the formation of longitudinal perturbations and their interaction with the ring vortices. Figure 2.9 shows that under the excitation, the three-dimensional deformations of the jet periphery become obviously stronger taking a mushroom-like shape. Thus, the acoustic forcing ensures more profound mixing of the jet with the surrounding air.

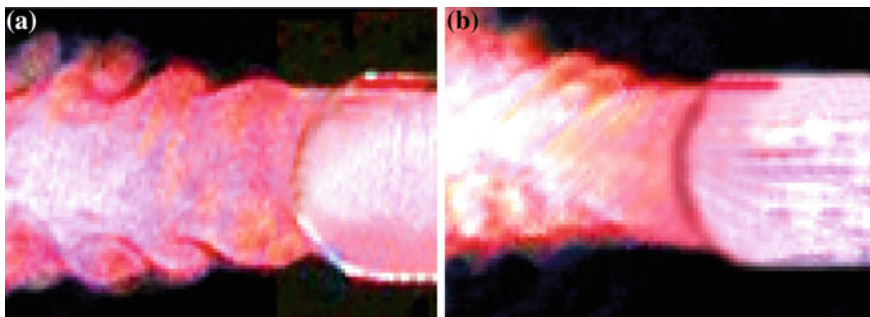


**Fig. 2.8** Acoustic effect on the ring vortices: excitation frequencies  $f = 110$  Hz (a) and  $f = 250$  Hz (b);  $U_0 = 5$  m/s



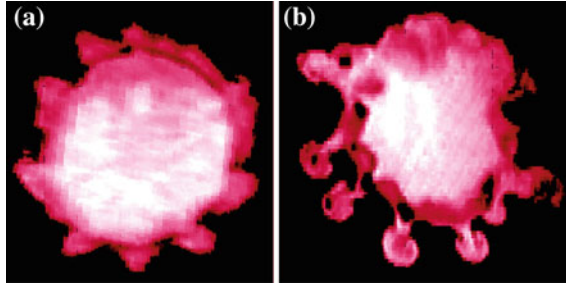


**Fig. 2.9** Visualization of the jet cross section  $x/d = 0.5$  without acoustic oscillations (a) and under the excitation at 140-Hz frequency and sound pressure level of 90 dB (b)

## 2.6 Effect of Flow Velocity on the Jet Evolution

Some flow patterns obtained in one and the same cross section of the jet are presented in Fig. 2.10 where one can trace the laminar flow breakdown at a fixed distance from the nozzle when increasing the flow velocity. The initial development of the three-dimensional perturbations (Fig. 2.10a, b), their interaction with the ring vortices resulting in the 3D bursts (Fig. 2.10c–f), and final transition to turbulence (Figs. 2.10g, h) are distinctly seen.

Finally, as criteria of the laminar and turbulent flow regimes the following can be taken. First, the hot-wire data on velocity perturbations at different streamwise stations (Fig. 2.2) show that the disturbances of the jet rapidly grow at  $x = 32$  mm (approximately four times comparing to their intensity at  $x = 8, 12$ , and  $22$  mm) as an indication of a transition to the turbulent state. Then, a chaotic motion typical of

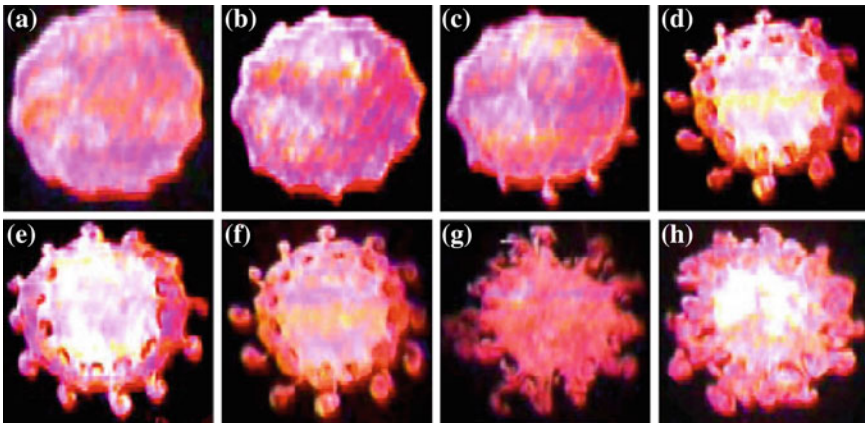


**Fig. 2.10** Visualization of the jet cross section  $x/d = 0.3$  at variation of flow velocity from  $U_0 = 6$  to 13 m/s with the step of 1 m/s (from a to h) (see Presentation Chap. 2: “Multimedia files Nos. 2.6, 2.8”) (<http://extras.springer.com>)

turbulent flow is seen in Figs. 2.4*h* and 2.10*h*, whereas in the upstream sections (Fig. 2.4*b–g*) and at a lower velocity of the jet core (Fig. 2.10*a–f*) an ordered flow structure is found that is typical of laminar flows and those at the early transitional stage.

### Key points

Summarizing the above experimental results, we focus on the following aspects of the laminar jet breakdown:

- The longitudinal structures of velocity perturbations contributing to the laminar flow breakdown can be generated close to the jet origin, i.e., the nozzle exit.
- Interaction of the ring vortices with the longitudinal disturbances is similar to the deformation of two-dimensional instability waves in a boundary layer by local flow non-uniformities.
- A result of the interaction is the generation of “beams” in the form of  $\Lambda$ - or  $\Omega$ -like structures spaced over the ring vortex.
- An intensive mixing of the jet with the surrounding air occurs in the region of the heads of  $\Lambda$ - or  $\Omega$ -like structures enhancing the jet spreading and its transition to the turbulent state.
- Under the external acoustic forcing, the passage frequency and the scales of the ring vortices are modified as well as mixing of the jet with ambient air becomes more profound.

### References

- Demare D, Baillot F (2001) The role of secondary instabilities in the stabilization of a nonpremixed lifted jet flame. *Phys Fluids* 13:2662–2669
- Klebanoff PS, Tidstrom KD, Sargent LM (1962) The three-dimensional nature of boundary layer instability. *J Fluid Mech* 12:1–34
- Van Dyke M (1986) *Album fluid motion*. Mir, Moscow, in Russian

Visualization of Conventional and Combusting Subsonic  
Jet Instabilities

Kozlov, V.; Grek, G.R.; Litvinenko, Y.

2016, XIV, 126 p. 133 illus., 14 illus. in color., Softcover

ISBN: 978-3-319-26957-3